Received 9 June 2006
Revised 23 November 2006
Accepted 13 February 2007

Mechanical and durability behaviour of growing concrete structures

Valentina A. Salomoni, Gianluca Mazzucco and Carmelo E. Majorana
Department of Construction and Transportation Engineering, Faculty of Engineering, University of Padua, Padua, Italy

Abstract

Purpose – This paper seeks to analyse 3D growing concrete structures taking into account the phenomenon of body accretion, necessary for the simulation of the construction sequence, and carbon dioxide attack.

Design/methodology/approach – A typical 3D segmental bridge made of precast concrete is studied through a fully coupled thermo-hygro-mechanical F.E. model. The durability of the bridge is evaluated and carbonation effects are considered. Creep, relaxation and shrinkage effects are included according to the theory developed in the 1970s by Bažant for concretes and geomaterials; the fluid phases are considered as a unique mixture which interacts with a solid phase. The porous material is modelled using n Maxwell elements in parallel (Maxwell-chain model).

Findings – First, calibration analyses are developed to check the VISCO3D model capabilities for predicting carbonation phenomena within concrete and the full 3D structure is modelled to further assess the durability of the bridge under severe conditions of CO_2 attack.

Originality/value – The adopted numerical model accounts for the strong coupling mechanisms of CO_2 diffusion in the gas phase, moisture and heat transfer, $CaCO_3$ formation and the availability of $Ca(OH)_2$ in the pore solution due to its transport by water movement. Additionally, the phenomenon of a sequential construction is studied and numerically reproduced by a sequence of "births" for the 3D finite elements discretizing the bridge. The fully coupled model is here extended to 3D problems for accreting bodies (as segmental bridges) in order to gather the effects of multi-dimensional attacks of carbon dioxide for such structures.

Keywords Concretes, Creep, Carbonation

Paper type Research paper

1. Introduction

Segmental bridges made of precast concrete are characterised by differential shrinkage and creep effects due to the construction sequence and corresponding addition of new concrete elements. As stated in van der Veen (2003), concrete segmental bridge design and construction is a complex process that must consider various time-dependant effects involving both materials and loading. From a material standpoint, concrete strength and deformation characteristics due to creep and shrinkage are all highly time dependent.

The aim of this paper is to further investigate the hygro-thermo-mechanical response of such 3D structures when deteriorated by carbonation phenomena. In fact, one of the main factors controlling the serviceability and safety performance of structural concrete is the corrosion of steel reinforcing bars (Ishida *et al.*, 2004). The passive layer around the steel bars naturally protects them from corrosion.

Engineering Computations: International Journal for Computer-Aided Engineering and Software
Vol. 24 No. 5, 2007
pp. 536-561

0264-4401
DOI 10.1108/02644400710755906

However, the penetration of carbon dioxide and the consumption of calcium hydroxide may cause a drop in the pH value of the pore water. Under low pH conditions (or in case of water dilution or in presence of corrosive anions), the thin oxide film around the steel surface is broken and it becomes unable to further protect the steel bars from corrosion. The most dangerous range of external relative humidity for carbonation is from 40 to 80 per cent, since the carbonation reaction calls for the presence of water, while under higher atmospheric humidity the diffusion of carbon dioxide will be inhibited by the water filling the pores (Saetta *et al.*, 1993). The corrosion initiation due to a carbonation process only is here investigated.

The numerical model accounts for the strong coupling mechanisms of CO_2 diffusion in the gas phase, moisture and heat transfer, $CaCO_3$ formation and the availability of $Ca(OH)_2$ in the pore solution due to its transport by water movement. Additionally, the phenomenon of a sequential construction is studied and numerically reproduced by a sequence of "births" for the 3D finite elements discretizing the bridge: the elements are sequentially activated with corresponding activation of their hygro-thermo-mechanical characteristics, including creep and shrinkage phenomena. This fully coupled model has already been presented elsewhere (Schrefler *et al.*, 1989; Saetta *et al.*, 1993, 1995; Majorana *et al.*, 1997, 1998; Majorana and Salomoni, 2004), but it is here extended to 3D problems for accreting bodies (as segmental bridges) in order to gather the effects of multi-dimensional attacks of carbon dioxide for such structures.

Creep, relaxation and shrinkage effects are dealt with according to the theory developed in the 1970s by Bažant (Bažant, 1972a, b; Bažant and Wu, 1974; Bažant and Wittmann, 1982; Bažant, 1982, 1988) for concretes and geomaterials; the fluid phases are considered as an unique mixture interacting with a solid phase. The porous material is modelled by n Maxwell elements in parallel (Maxwell-chain model).

The problem of accretion (boundary value problem) is treated according to Arutiunian (1976a, b) and Arutiunian (1977) with elements of different ages superimposed to create the whole structure in a discrete way. In Bugakov (1973), the problem of mass growing is solved through methods of the elasticity theory, whereas in Naumov (1994) the theory of a viscoelastic body is used in order to consider the stress and strain states in homogeneous growing bodies. A more general formulation is used for the same problem in Diatlovitskii and Vainberg (1975).

2. Thermo-hygro-mechanical model

The field equations of the model are briefly recalled below; for additional details, the reader is referred to the u-h-T model presented in Schrefler *et al.* (1989), further extended in Majorana *et al.* (1997, 1998).

The model consists of a mass conservation equation in terms of relative humidity, an energy conservation equation and the linear momentum balance equation for the multiphase material. Improvements are introduced to take into account carbon dioxide flows within a 3D porous material. Creep and shrinkage effects are evaluated according to the theory by Bažant, as previously stated.

The coupled system of differential equations for dealing with humidity diffusion and heat transport can be written in the form (Majorana, 1985; Schrefler *et al.*, 1989; Majorana *et al.*, 1998):

$$\frac{\partial h}{\partial t} - \nabla^{\mathrm{T}}\mathbf{C}\nabla h - \frac{\partial h_{\mathrm{s}}}{\partial t} - k\frac{\partial T}{\partial t} + \bar{\alpha}\mathbf{m}^{\mathrm{T}}\frac{\partial \varepsilon}{\partial t} = 0$$
$$\rho C_{\mathrm{q}}\frac{\partial T}{\partial t} - \nabla^{\mathrm{T}}\mathbf{\Lambda}\nabla T - \frac{\partial Q_{\mathrm{h}}}{\partial t} = 0 \tag{1}$$

where $\mathbf{C}$ is the (relative humidity) diffusivity diagonal matrix, $\mathrm{d}h_{\mathrm{s}}$ self-dessication, k hygrothermic coefficient, $\bar{\alpha} = \left(\partial h/\partial \varepsilon_{\mathrm{v}}\right)\big|_{T,w}$ equals the change in h due to unit change of volumetric strain ε_{v} at constant moisture content w, ρC_{q} is the thermal capacity, ($\mathbf{\Lambda}$ thermal conductivity diagonal matrix and Q_{h} outflow of heat per unit volume of solid.

Once carbonation phenomena are accounted for, the above system becomes (Saetta *et al.*, 1993, 1995):

$$\frac{\partial h}{\partial t} = \nabla^{\mathrm{T}}\mathbf{C}\nabla + \frac{\partial h_{\mathrm{s}}}{\partial t} + k\frac{\partial T}{\partial t} - \bar{\alpha}\mathbf{m}^{\mathrm{T}}\frac{\partial \varepsilon}{\partial t} + \frac{\partial h_{\mathrm{c}}}{\partial t}$$
$$\rho C_{\mathrm{q}}\frac{\partial T}{\partial t} = \nabla^{\mathrm{T}}\mathbf{\Lambda}\nabla T + \frac{\partial Q_{\mathrm{h}}}{\partial t} + \frac{\partial T_{\mathrm{c}}}{\partial t} \tag{2}$$
$$\frac{\partial c}{\partial t} = \nabla^{\mathrm{T}} D_{\mathrm{c}}\nabla c - \frac{\partial c_{\mathrm{c}}}{\partial t}$$

where c and D_{c} are the carbon dioxide concentration and diffusivity, and $\partial h_{\mathrm{c}}/\partial t$, $\partial T_{\mathrm{c}}/\partial t$, $\partial c_{\mathrm{c}}/\partial t$ are, respectively, the changes of relative humidity, temperature and CO_2 concentration due to carbonation in a unit of time.

Equations (1) and (2) are complemented in the model by the equilibrium equation and the constitutive relationship (Schrefler *et al.*, 1989; Majorana *et al.*, 1998).

According to what has been presented in Papadakis *et al.* (1991) and Ishida *et al.* (2004) and experimentally observed, it can be assumed (for comparison purposes) that the time history for the carbon dioxide diffusivity can proceed in agreement with:

$$D_{\mathrm{c}} = A_{\mathrm{c}}\frac{y}{t}\ \ y = \alpha_{\mathrm{c}} t^{-1/2}\ \ D_{\mathrm{c}} = A_{\mathrm{c}}\alpha_{\mathrm{c}} t^{-1/2} \text{ for } D_c < 1.5A_{\mathrm{c}}\ \ D_{\mathrm{c}} = 1.5A_{\mathrm{c}} \text{ for } D_{\mathrm{c}} \geq 1.5A_{\mathrm{c}} \tag{3}$$

in which A_{c} has the dimension of a square length for unit time (material parameter), t is the exposure time and α_{c} is carbonation rate coefficient, depending on both w/c ratio and CO_2 concentrations. This assumption can be motivated by the observation (Papadakis *et al.*, 1991; Houst and Wittmann, 1994) that the micropore structure of cementitious materials may change due to carbonation. In fact, a proposed formula for the porosity variation can be expressed as (Ishida *et al.*, 2004):

$$\Phi' = \alpha\Phi \tag{4}$$

where Φ' is the porosity after carbonation, Φ porosity before carbonation, α a reduction parameter. Hence, a reduction in porosity corresponds to a reduction in carbon dioxide diffusivity. So, the variation of the latter can be initially linked to the carbonation velocity which decreases with time (Ishida *et al.*, 2004) and to the constant A_{c} (equation (3)); once a specific time station is reached, the diffusivity becomes constant with time. In this way, the decrease in CO_2 velocity, due to the increasing carbonation of the material exposed to carbon dioxide aggression, is simulated.

Creep and relaxation processes are modelled by n Maxwell elements in parallel (Maxwell-chain model) (Bažant and Wu, 1974; Bažant and Wittmann, 1982), as shown Figure 1.

The time-dependent nature of the constitutive law is expressed in integral form as:

$$\sigma(t) = \int_0^t R(t, t')\mathbf{D}'\mathrm{d}\varepsilon(t') \tag{5}$$

where:

$$\mathbf{D}'^{-1} = \begin{bmatrix} 1 & -\nu & -\nu & 0 & 0 & 0 \\ & 1 & -\nu & 0 & 0 & 0 \\ & & 1 & 0 & 0 & 0 \\ & & & 2(1+\nu) & 0 & 0 \\ & & & & 2(1+\nu) & 0 \\ & & & & & 2(1+\nu) \end{bmatrix} \tag{5a}$$

As proved above, the time-dependent stress-strain relationship requires the knowledge of the function $R(t,\ t')$, called relaxation function which, in accordance with the Maxwell-chain model, can be expressed in its degenerate form (Majorana and Vitaliani, 1990) (to overcome the difficulties connected with the numerical integration of equation (5)) as:

$$R(t, t') = \sum_{\mu=1}^{n} E_\mu(t')\mathrm{e}^{-((t-t')/\tau_\mu)} \tag{6}$$

where t' is the time of first application of load and τ_μ relaxation times.

Generally, another function $J(t,t')$ called creep function and dual to $R(t,t')$ is more simply derived from experiments compared to the relaxation function: the former is complementary to the latter and it relates strains to stresses through

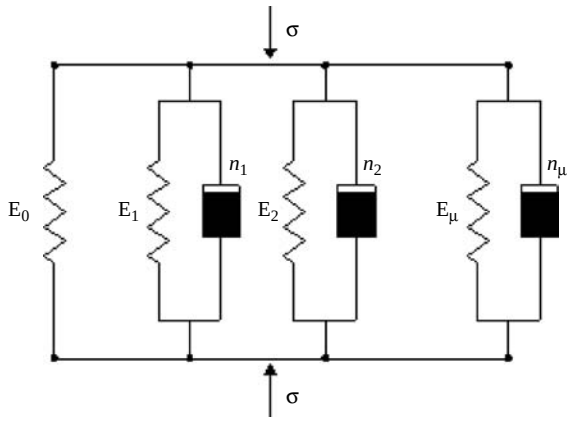

Figure 1.
n Maxwell elements in parallel

an expression similar to equation (5). A typical expression for the creep function in its degenerate form is:

$$J(t,t') = \sum_{\mu=1}^{N} \frac{1}{C_\mu(t')} \left\{1 - \exp[y_\mu(t') - y_\mu(t)]\right\} \tag{7}$$

where the functions $y_\mu(t)$ are called reduced times and may be expressed as:

$$y_\mu(t) = \left(\frac{t}{\tau_\mu}\right)^{q_\mu} \quad (\mu = 1, 2, \ldots N) \tag{8}$$

where q_μ are positive exponents ≤ 1 and E_μ, C_μ represent the μ-th elastic modulus of the Maxwell unit and the specific creep, respectively. For a complete description of the model, the reader is referred to (Majorana, 1985; Majorana and Vitaliani, 1990; Majorana *et al.*, 1997, 1998).

However, it is to be underlined that the described approach for simulating aging viscoelasticity through a rate-type aging constitutive model (equations (6)–(8)) suffers from some weaknesses, among which the fact that different retardation times can give almost equally good fits of the measured creep curves: a simple method to determine the (discrete) retardation spectrum has been available in Bažant and Prasannan (1989a, b) for creep curves in the form of the power law, log-law, or log-power law. These shortcomings are in fact avoided by the solidification theory, through which aging is entirely due to the growth of the volume fraction of the load-bearing solidifying matter (hydrated cement), which itself is non-aging. By separating aging in the form of volume growth from the viscoelastic behaviour, it is possible to describe creep by a Kelvin chain with age-independent properties; according to these studies, E_μ takes the form:

$$E_\mu = \frac{1}{q_2 A_\mu} = \frac{1}{q_2 b_\mu(n)(\tau_1 10^{\mu-1})^{m(\mu)}}, \quad m(\mu) = \frac{n}{1 + (c\mu)^z} \tag{9}$$

where n is the exponent of a power function, $b_\mu(n)$, c and z have been optimized by using a computer library subroutine for Levenberg-Marquardt algorithm (Bažant and Prasannan, 1989b) and q_2 is an empirical material constant (Bažant and Kim, 1991).

But even this approach has a validity restricted to the log-power law and in general, when a slightly different creep law is required, it fails.

Hence, to deal with general creep laws and to avoid the aforementioned weak points including the nonuniqueness, an effective approach is to introduce within the solidification theory the continuous Kelvin chain model with infinitely many Kelvin units and retardation times spaced infinitely closely, for which A_μ becomes a continuous retardation spectrum (Bažant and Xi, 1993, 1994). Such a spectrum may be evaluated by a certain method developed in the theory of viscoelasticity (Tschoegl, 1971; Tschoegl, 1989) and the Widder's inversion formula (Widder, 1971). For the compliance function of the non-aging constituent, the log-power creep law is assumed (Bažant and Xi, 1993, 1994):

$$J(t,t') = q_2 \ln\left[1 + \left(\frac{t - t'}{\lambda_0}\right)^n\right] \tag{10}$$

in which $\lambda_0 = 1$ day can be taken for most concretes. When $J(t,t')$ has the form of equation (7), i.e.:

$$J(t,t') = \sum_{\mu=1}^{N} A_\mu [1 - e^{-((t-t')/\tau_\mu)}] \tag{11}$$

A_μ becomes (approximating):

$$A_\mu = \ln 10 q_2 n(n-1) \frac{(3\tau_\mu)^n}{1 + (3\tau_\mu)^n} \tag{12}$$

which gives the simplified continuous spectrum. It is proved (Bažant and Xi, 1993) that the creep functions obtained from the continuous spectrum agree with the log-power curve very well and additionally the continuous retardation spectrum is able to reflect the creep intensity in various time ranges.

A similar approach has been developed in Bažant and Zi (2002) to determine the continuous relaxation spectrum for the Maxwell chain model, approximately calculated from equation (10) simply by algebraic inversion, viz.:

$$R(t,t') = \frac{1}{J(t,t')} \tag{13}$$

Additionally, both the drying creep effect and the long-time aging of creep compliance can be more realistically and more generally represented by relaxation of microprestress (Bažant and Zi, 2002; Bažant *et al.*, 1997; Bažant, 2001), which is justified by the fact that the solidification theory alone is unable to explain long-term aging because the volume growth of the hydration products is too short-lived. This phenomenon can be explained by relaxation of a tensile microprestress in the bonds or bridges across the micropores in hardened cement gel filled by hindered adsorbed water. Then, the amalgamation of microprestress and solidification models leads to a compliance function of concrete expressed as:

$$J(t,t') = J^*(t,t') + q_4' S^{p-1} \tag{14}$$

in which $J^*(t,t')$ is the viscoelastic compliance affected by the volume growth of hydration products (in agreement with the solidification theory), q_4' is an empirical function, p a constant ($p > 1$; in numerical simulations, the value of $p = 2$ can be taken) and S indicates the relaxing microprestress, given by, in case of no drying or wetting:

$$S = S_0 \left(\frac{t_0}{t} \right) \tag{15}$$

with S_0 initial value of S at time t_0; on the contrary, in the limiting case of maximum h variations:

$$S = -c_1 \ln h + \text{const.} \tag{16}$$

where c_1 is a constant.

Hence, the rate-type aging constitutive model here adopted (already implemented in the VISCO3D F.E. code) will be updated accordingly in a future paper; however, firstly, it is the authors' conviction that the new results would not change significantly; secondly, the aim now is to analyse the 3D thermo-hygro-mechanical response of an accreting body and the consequent mutual effects, particularly on the hygro-thermal regime of each structural segment.

3. Mesh accretion – the boundary value problem

References Arutiunian (1976a, b, 1977) are used as basis for the formulation of the boundary value problem of the theory of creep in a 3D non-uniform aging body with elements of different ages superimposed to create the whole structure in a discrete way. The equations of state for non-uniform aging bodies (Arutiunian, 1977) occupying, prior the merging, the region $\Omega^{(i)}$ and loaded at the time instant τ_i^0 can be written, according to Arutiunian (1976a, b), in the form:

$$\begin{aligned}
\varepsilon_{\alpha\beta}^{(i)}(\underline{r},t) &= \varepsilon_{\alpha\beta}^{0(i)}(\underline{r},t) + (1+\nu)\left[\left(I+L^{(i)}\right)\frac{\sigma_{\alpha\beta}^{(i)}}{E}\right] - \nu\delta_{\alpha\beta}\left[\left(I+L^{(i)}\right)\frac{\sigma_{SS}^{(i)}}{E}\right] \\
\sigma_{\alpha\beta}^{(i)}(\underline{r},t) &= \frac{E(t-\tau_i^*)}{1+\nu}\left\{\left(I+N^{(i)}\right)\left[\varepsilon_{\alpha\beta}^{(i)} - \varepsilon_{\alpha\beta}^{0(i)}\right]\right. \\
&\quad \left. +\delta_{ij}\frac{\nu}{1-2\nu}\left(I+N^{(i)}\right)\left[\varepsilon_{SS}^{(i)} - \varepsilon_{SS}^{0(i)}\right]\right\} \\
I\left(\frac{\sigma_{\alpha\beta}^{(i)}}{E}\right) &= \frac{\sigma_{\alpha\beta}^{(i)}(\underline{r},t)}{E\left(t-\tau_i^*\right)} \\
L^{(i)}\left(\frac{\sigma_{\alpha\beta}^{(i)}}{E}\right) &= \int_{\tau_i^0}^{t}\frac{\sigma_{\alpha\beta}^{(i)}(\underline{r},t)}{E\left(\tau-\tau_i^*\right)}J(t-\tau_i^*,\tau-\tau_i^*)\mathrm{d}\tau \\
N^{(i)}\left(\varepsilon_{\alpha\beta}^{(i)}\right) &= \int_{\tau_i^0}^{t}\varepsilon_{\alpha\beta}^{(i)}(\underline{r},t)R(t-\tau_i^*,\tau-\tau_i^*)\mathrm{d}\tau
\end{aligned} \tag{17}$$

where ν is the Poisson's ratio, $\delta_{\alpha\beta}$ the Kronecker delta, $\varepsilon_{\alpha\beta}^{0(i)}$ denotes the assumed (thermo-hygrometric) deformations and E, J, R are the moduli of instantaneous elastic deformation, the creep kernel and the relaxation kernel, respectively, of the material of the body which occupies the region $\Omega^{(i)}$, produced at the time instant τ_i^*.

The basic assumption concerning the merging of the body is that no discontinuities have to appear both in the displacements of the body during the time interval between two subsequent mergings and in the stress vector $\boldsymbol{\sigma}_n$ at the contact surface. The condition of continuity is:

$$u_\alpha(\underline{r},t) = u_\alpha(\underline{r},t_m) + \Delta^{(m)}u_\alpha(\underline{r},t) \tag{18}$$

The equation connecting deformations and displacements after merging, namely at $t_m \le t \le t_{m+1}$, is, according to equation (18):

$$\varepsilon_{\alpha\beta}(\underline{r},t)=\varepsilon_{\alpha\beta}(\underline{r},t_m)+\frac{1}{2}\left[\Delta^{(m)}u_{\alpha,\beta}(\underline{r},t)+\Delta^{(m)}u_{\beta,\alpha}(\underline{r},t)\right] \tag{19}$$

where $\Delta^{(m)}u_\alpha$ denotes the displacement increments satisfying the conditions of continuity in the region $\Omega(t)$ for $t_m \le t \le t_{m+1}$.

Let us indicate the boundary of $\Omega(t)$ by $S(t)$ and let this boundary consists of five segments $S(t)=S_0(t)\cup S_1(t)\cup S_2(t)\cup S_3(t)\cup S_4(t)$.

Hence, the equations of quasi-static equilibrium and the boundary conditions in terms of stresses and displacements, written at times $t_m \le t \le t_{m+1}$, take the form:

$$\sigma_{\alpha\beta,\beta}(r,t)+f_\alpha(r,t)=0,\ \underline{r}\in\Omega(t)\ \ \sigma_n(r,t)=0,\ \underline{r}\in S_0(t)\ \ \underline{\sigma}_n(r,t)=\underline{F}(r,t),\ \underline{r}\in S_1(t) \tag{20}$$

$$\begin{gathered}\underline{u}(\underline{r},t)=\underline{V}(\underline{r},t),\ \ \underline{r}\in S_2(t)\quad u_n(\underline{r},t)=V_n(\underline{r},t),\ \underline{\sigma}_\tau(\underline{r},t)=\underline{F}_\tau(\underline{r},t),\ \ \underline{r}\in S_3(t)\\ \sigma_n(\underline{r},t)=F_n(\underline{r},t),\ \underline{u}_\tau(\underline{r},t)=\underline{V}_\tau(\underline{r},t),\ \ \underline{r}\in S_4(t)\end{gathered} \tag{21}$$

The equation of state of the creep theory connecting the tensors $\boldsymbol{\varepsilon}_{\alpha\beta}(r,t)$ and $\boldsymbol{\sigma}_{\alpha\beta}(r,t)$ has the expression:

$$\begin{gathered}\boldsymbol{\varepsilon}_{\alpha\beta}(\underline{r},t)=(1+\nu)[I+L]\left(\frac{\sigma_{\alpha\beta}}{E}\right)-\nu\delta_{\alpha\beta}[I+L]\left(\frac{\sigma_{SS}}{E}\right)+\varepsilon^0_{\alpha\beta}(\underline{r},t)\\ \boldsymbol{\sigma}_{\alpha\beta}(\underline{r},t)=\frac{E\left[t-\chi(\underline{r})\right]}{1+\nu}\left\{(I+N)\left(\boldsymbol{\varepsilon}_{\alpha\beta}-\varepsilon^0_{\alpha\beta}\right)+\delta_{\alpha\beta}\left(\frac{\nu}{1-2\nu}\right)(I+N)\left(\boldsymbol{\varepsilon}_{SS}-\boldsymbol{\varepsilon}^0_{SS}\right)\right\}\\ I\left(\frac{\sigma_{\alpha\beta}}{E}\right)=\frac{\sigma_{\alpha\beta}(\underline{r},t)}{E\left[t-\chi(\underline{r})\right]}\ L\left(\frac{\sigma_{\alpha\beta}}{E}\right)=\int_{\gamma(\underline{r})}^{t}\frac{\sigma_{\alpha\beta}(\underline{r},\tau)}{E\left[\tau-\chi(\underline{r})\right]}J[t-\chi(\underline{r}),\tau-\chi(\underline{r})]\mathrm{d}\tau\\ N(\varphi)=\int_{\gamma(\underline{r})}^{t}R[t-\chi(\underline{r}),\tau-\chi(\underline{r})]\varphi(\underline{r},\tau)\mathrm{d}\tau\end{gathered} \tag{22}$$

in which $\gamma(\underline{r})=\tau_i^0$, $\chi(\underline{r})=\tau_i^*$ and $R[t-\chi(\underline{r}),\tau-\chi(\underline{r})]$ is a resolvent of the creep kernel $J[t-\chi(\underline{r}),\tau-\chi(\underline{r})]$.

The system of equations consisting of equation (19), the first equation of (20) and the first equation of (22) with the boundary conditions (21), represents a closed system which leads to determine the solution of the boundary value problem of the creep theory for non-uniform aging bodies undergoing incremental growth. So its solution will automatically satisfy the usual conditions of continuity of the displacements, deformations and stresses at the boundary surface between the component bodies (Bugakov, 1973). The jumps in the values of the stress field components at the surface S_{ij} can be determined by solving the boundary value problem consisting of equation (19), the first equation of (20) and the conditions (21). The formulation of the boundary value problem under the hypotheses of continuous growth is shown in Diatlovitskii and Vainberg (1975) and Naumov (1994).

3.1 Numerical formulation

The numerical procedure reproducing the above discrete growth consists in introducing the whole body (structure) of volume V at time $t = 0$, characterised by elements of volume V_m, so that:

$$V = V_1 \cup V_2 \ldots \cup V_{m\ldots} \cup V_k \tag{23}$$

Accretion is obtained first "blocking" all the material properties (thermal, hygral and mechanical) of those parts of the body which do not exist at $t = 0$; hence, at $t = 0 + t_1$, $V = V_1$, whereas the others V_i ($i = 2, \ldots$ k) are present but "dead" (birth and death procedure).

Our study, being mainly concentrated on creep phenomena, suggests that the values of E_μ (Bažant and Wu, 1974) for the dead elements are fixed, so that:

$$C_\mu = E_\mu \frac{\dot{y}(t)}{\dot{y}(t) - 1} \rightarrow \infty \Rightarrow J(t, t') \rightarrow 0 \tag{24}$$

and the evolution of creep is avoided.

Further, once time t_m (when the body V_m is connected to V) is reached, all the material characteristics of V_m are activated, including boundary conditions. Continuity is respected on the contact surfaces, in terms of both stress and strain (Figure 2).

Activation means triggering of humidity variations, concrete desiccation and/or heat transfer due to temperature gradients. Any boundary condition is activated for $t \geq t_m$ only (Figure 3).

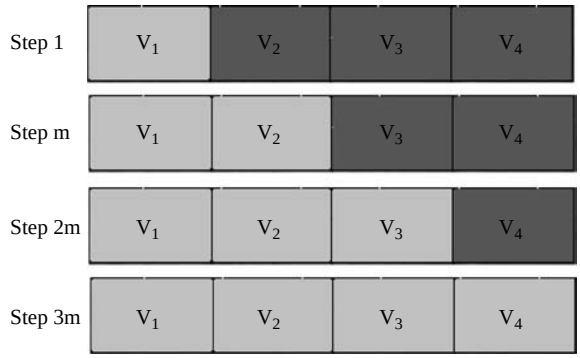

Figure 2.
Schematic of the incremental procedure for elements' birth

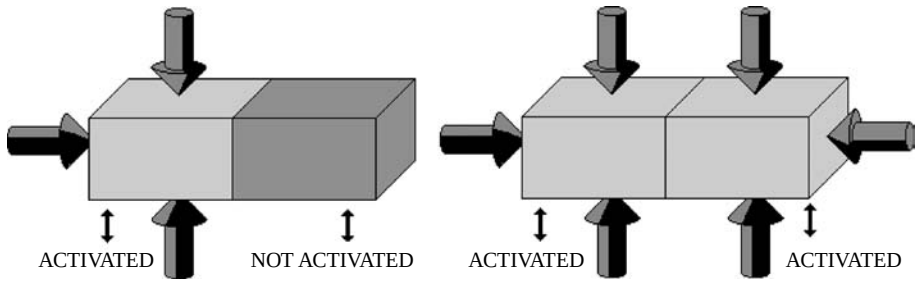

Figure 3.
Schematic of BCs' activation

4. Durability – the carbonation process

As previously indicated, the prime effect of carbonation within concrete pastes is to decrease their pH, creating conditions for steel bars oxidation. As secondary effects, CO_2 can generate leaching (not discussed here) or influence shrinkage (Collepardi, 1980). In fact, if carbon dioxide comes into contact with concrete after it has shrunk by desiccation, an additional shrinkage appears. This is due to the transformation of CO_2 into carbonic acid H_2CO_3 which reacts with calcium hydroxide $Ca(HO)_2$ generating calcium carbonate $CaCO_3$ and water.

The reaction is described by (Collepardi, 1980):

$$H_2CO_3 + Ca(OH)_2 \rightarrow CaCO_3 + 2H_2O \tag{25}$$

The basic nature of concrete comes from the generation of $Ca(OH)_2$, so that a thick film of Fe(OOH) is formed around the steel bars, passivating them against corrosion; steel is hence subjected to further oxidation from oxygen if the pH value of the pore water decreases. This drop may be caused by a further penetration of carbon dioxide and the consumption of calcium hydroxide; however, if concrete pores are filled with water, the penetration of carbon dioxide is hindered due to the low rate of diffusion of CO_2 in water while, if the pores are completely dry, the reaction of carbon dioxide with water molecules is absent. However, depassivation can also happen by water dilution and corrosive anions (e.g. chlorides) (Bažant, 1979a, b).

In the following, we will consider the corrosion initiation due to a carbonation process only; the corrosion propagation (depending on the rate of diffusion of oxygen and water) is not treated here, considering the initiation period as representative for a first durability assessment of the structure.

Hence, if concrete had RH = 100 per cent, pores would be saturated and carbon dioxide, being unable to penetrate, would not activate the reaction; differently, with RH = 0 per cent, carbon dioxide would penetrate quickly but it could not react with water to form the carbonic acid triggering the carbonation process. This explains why the carbonation phenomenon occurs mainly within a (internal) relative humidity range of 50-80 per cent, with maximum effects in the former scenario.

For a complete explanation of the processes of corrosion, the reader is referred to (Bažant, 1979a, b).

4.1 Assessment of the carbonation depth

As previously stated, the progression with time of the carbonated front (carbonation depth) depends on a variety of factors, e.g. water-cement ratio w/c, time, temperature T, porosity, external relative humidity, atmospheric CO_2 concentration.

Some authors (Papadakis *et al.*, 1991; Ishida *et al.*, 2004) experimentally obtained the depth of carbonation, being a function varying with the square root of exposure time under the form (for a Portland cement concrete), see equation (3):

$$y_d = \alpha_c \sqrt{t} \tag{26}$$

At constant (environmental) RH = 55 per cent, a series of values for α_c (independent on time) were obtained, as listed in Table I and shown in Figure 4. The α_c^1/α_c^2 ratio allows for converting the time scale in accelerated environments into the time scale under normal conditions (Ishida *et al.*, 2004): generally speaking, the accelerated test underestimates the resistance to carbonation of lower w/c concretes.

Using the values reported in (Ishida *et al.*, 2004) (RH = 55 per cent, $w/c = 0.6$, $T = 20$°C, CO_2 concentration = 10 per cent; in the following these results are addressed as "BC_1") for a 1D case, the curves of Figures 5 and 6 for the carbonation depth and velocity were obtained, for a time scale of years and days, respectively.

Table I.
Calculated carbonation rate coefficients for different atmospheric CO_2 concentrations

w/c (per cent)	α_c^1 (mm/years$^{1/2}$) ($CO_2 = 10$ per cent)	α_c^2 (mm/years$^{1/2}$) ($CO_2 = 0.07$ per cent)	α_c^1/α_c^2
80	79.1	10.8	7.32
60	51.2	6.8	7.53
40	23.9	3.0	7.79

Source: Ishida *et al.* (2004)

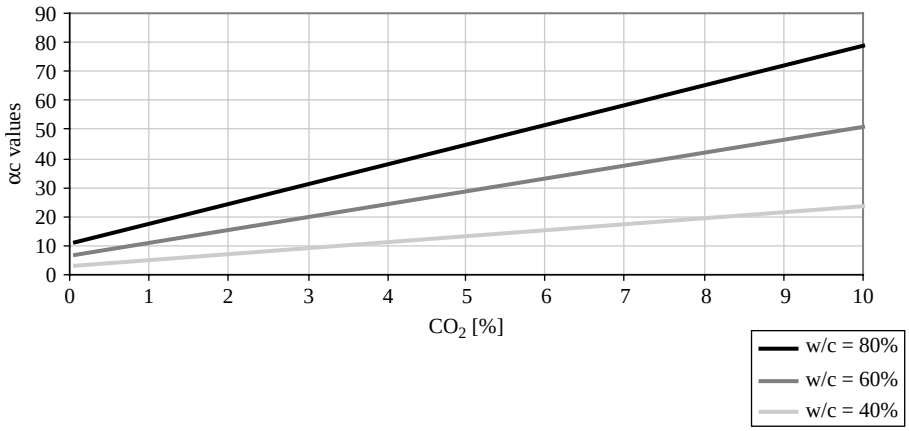

Figure 4.
Curves of α_c coefficient (equation (26))

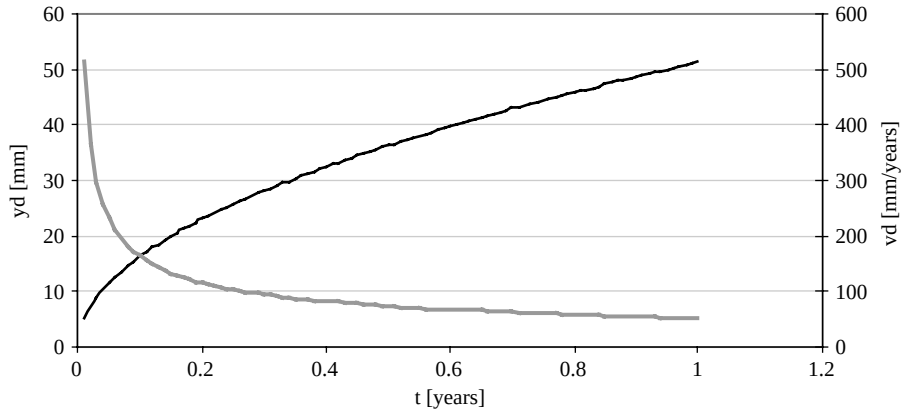

Figure 5.
History of carbonation depth and velocity (in years)

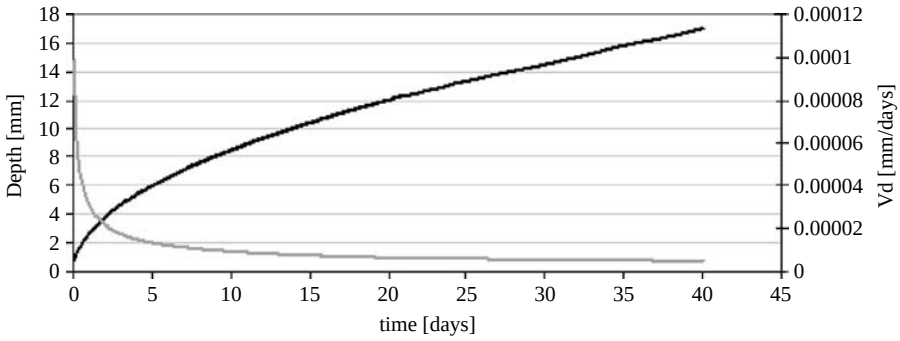

Figure 6.
History of carbonation depth and velocity (in days)

4.2 Calibration of the model

First, some calibration analyses were performed on a 3D sample to check the model capabilities of fitting available experimental data, hence ensuring realistic predictions for durability assessments of concrete structures and particularly concrete segmental bridges. Whereas the curves of Figure 7 come from equation (26) and fit the results obtained in Ishida *et al.* (2004) (dots) (the latter are shown in Figure 8 (crosses) at different time stations), with the values reported in the previous section (BC_1; Table II), the results shown in Figures 8 and 9 (contour maps) were obtained in terms of carbonation (per cent) vs depth for different times. The difference among results is justified by the three-dimensionality of our analyses versus the one-dimensionality of

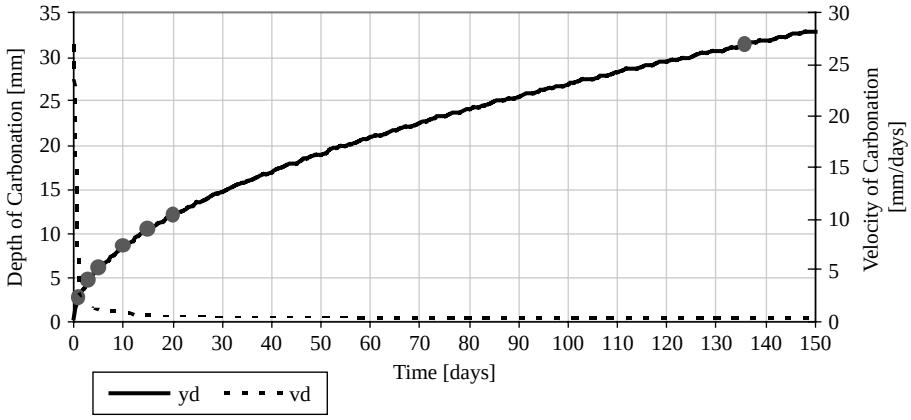

Figure 7.
Carbonation depth and velocity for BC_1

Note: The dots indicate the results from Ishida et al. (2004)

Day	1	3	5	10	15	20	136
Depth (mm)	2.69	4.67	6.03	8.52	10.44	12.06	31.44

Source: Ishida *et al.* (2004)

Table II.
Experimental results for carbonation depth with BC_1

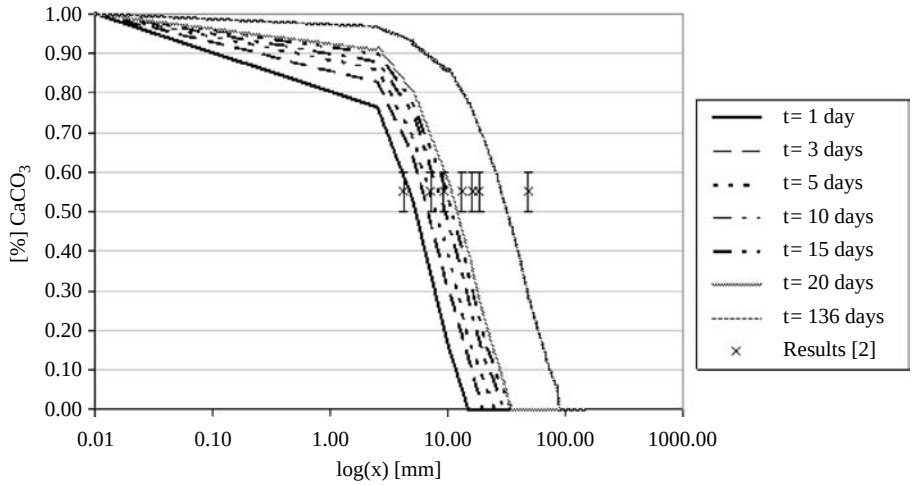

Figure 8.
$CaCO_3$ variation along the sample at different times ($w/c = 0.6$)

Ishida *et al.* (2004): hence, a 1D analysis generally overestimates (if the 3D body surface is convex) the carbonation velocity at higher w/c ratios (Figure 9).

A second test was performed, with BCs given by RH = 55 per cent, $w/c = 0.4$, $T = 20°C$, CO_2 concentration = 10 per cent (BC_2), whose experimental results are listed in Table III. The numerical results are shown in Figures 10 and 11 (contour maps) in terms of carbonation (per cent) vs depth for different times, whereas the curves of Figure 12 come again from equation (26).

Being the w/c ratio decreased, the carbonation depth is reduced; in fact, a lower w/c value generates a reduction in the concrete pores and consequently a decrease in CO_2 (and therefore $CaCO_3$) velocity.

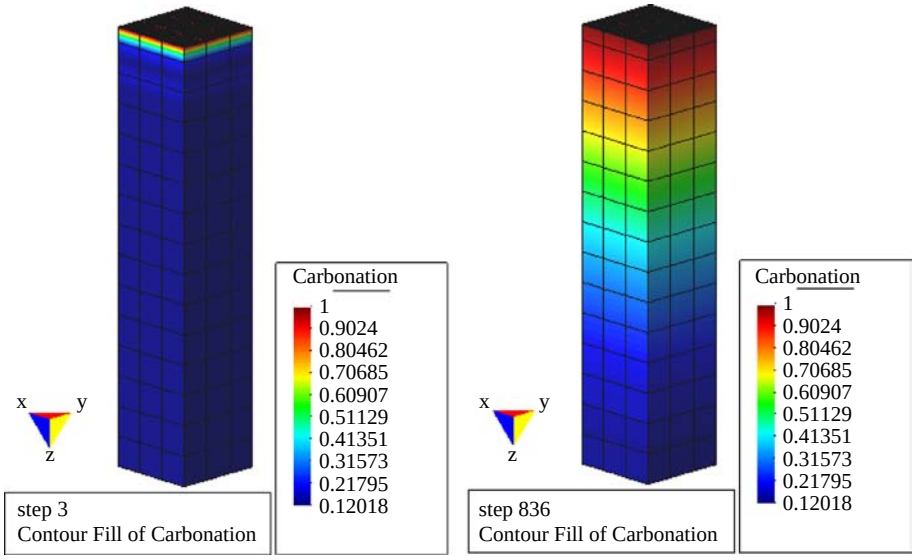

Figure 9.
Progression of the carbonated front after 0.2 (left) and 836 (right) days ($w/c = 0.6$)

The last test considers BCs given by RH = 55 per cent, $w/c = 0.8$, $T = 20°C$, CO_2 concentration = 10 per cent (BC_3), whose experimental results are listed in Table IV; Figure 13 represents equation (26), whereas the numerical results are shown in Figures 14 and 15 (contour maps) in terms of carbonation (per cent) vs depth for different times.

Day	1	3	5	10	15	20	136
Depth (mm)	1.25	2.17	2.80	3.96	4.85	5.59	14.59

Source: Ishida *et al.* (2004)

Table III.
Experimental results for carbonation depth with BC_2

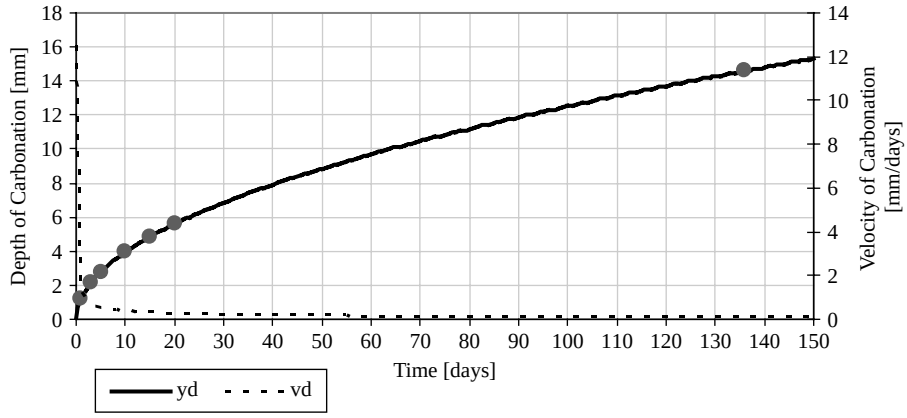

Note: The dots indicate the results from Ishida et al. (2004)

Figure 10.
Carbonation depth and velocity for BC_2

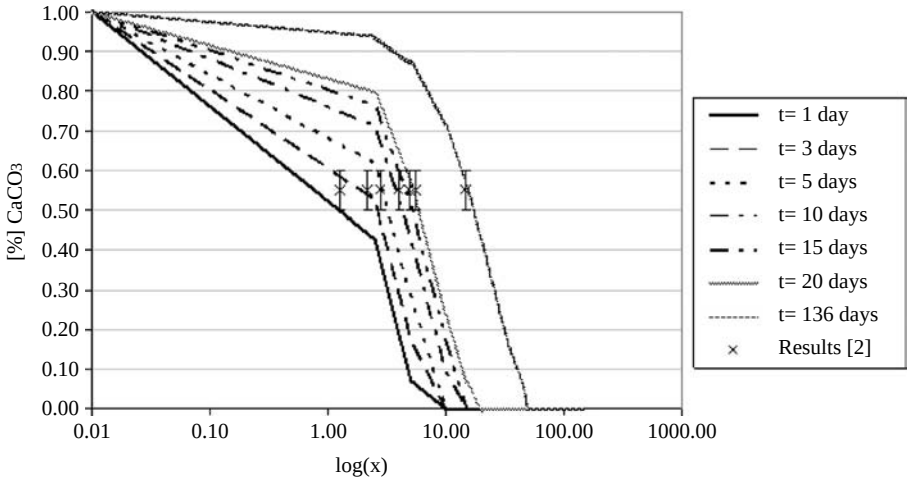

Figure 11.
$CaCO_3$ variation along the sample at different times ($w/c = 0.4$)

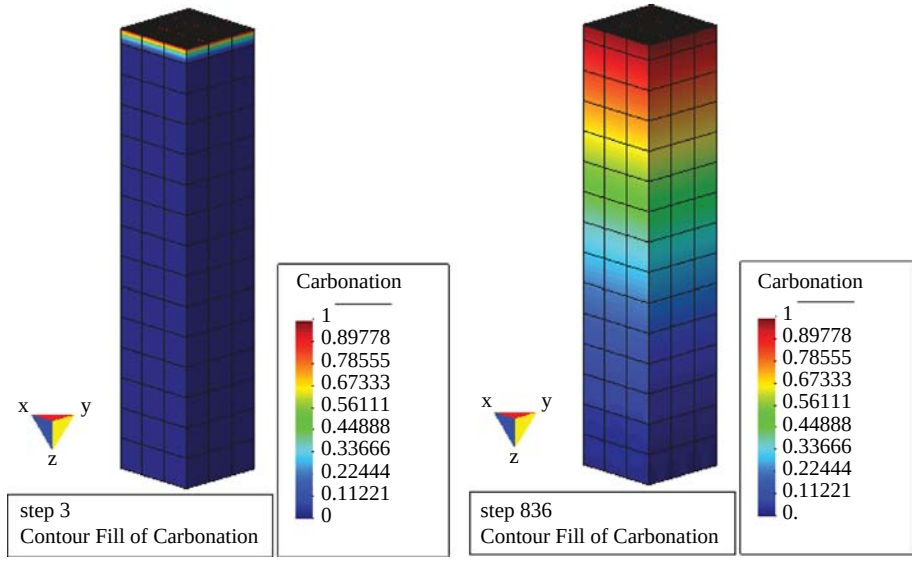

Figure 12.
Progression of the carbonated front after 0.2 (left) and 836 (right) days ($w/c = 0.4$)

Table IV.
Experimental results for carbonation depth with BC_3

Day	1	3	5	10	15	20	136
Depth (mm)	4.14	7.17	9.26	13.09	16.04	18.52	48.28

Source: Ishida *et al.* (2004)

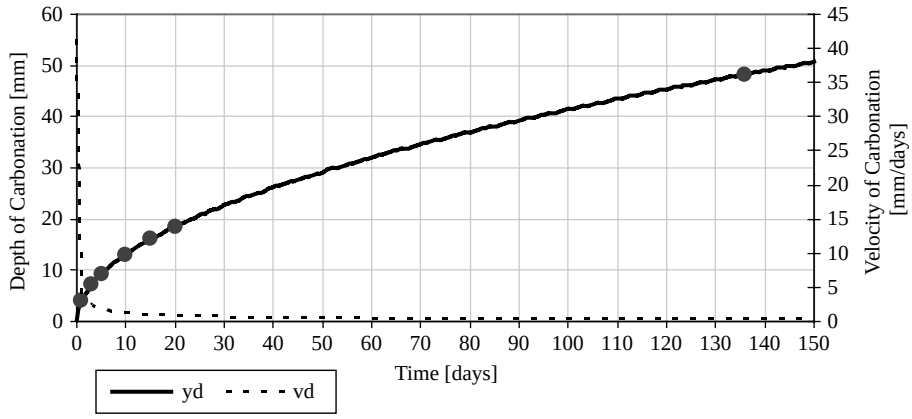

Figure 13.
Carbonation depth and velocity for BC_3

Note: The dots indicate the results from Ishida et al. (2004)

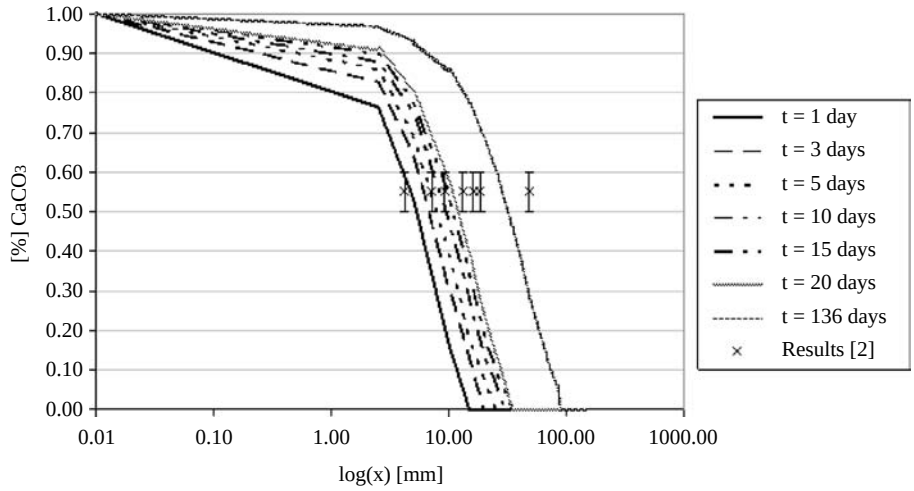

Figure 14.
$CaCO_3$ variation along the sample at different times ($w/c = 0.8$)

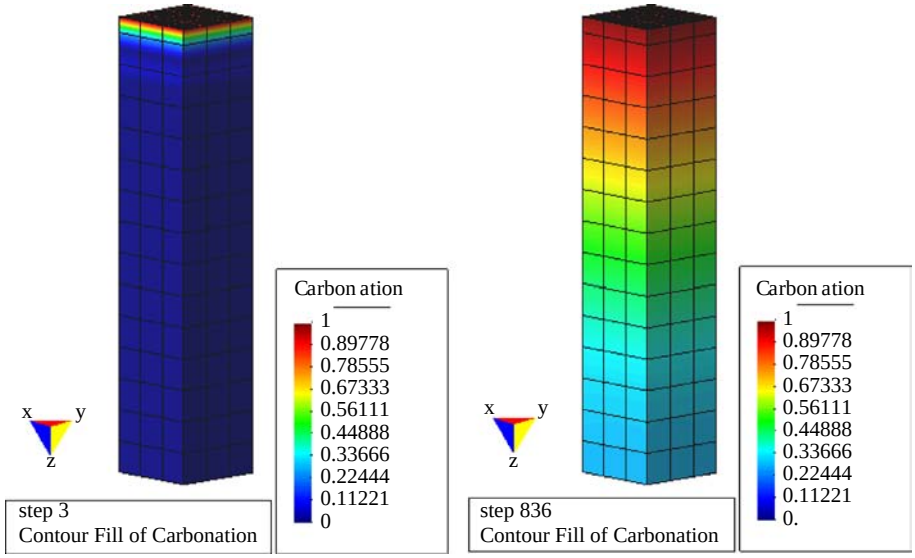

Figure 15.
Progression of the carbonated front after 0.2 (left) and 836 (right) days ($w/c = 0.8$)

It can be observed that such a w/c ratio determines the most dangerous situation for concrete: in fact, as shown by Figure 14, the carbonation front penetrates the sample more quickly than when lower ratios are considered.

5. Application (3D segmental bridge)

A typical highway viaduct was modelled to study the coupled phenomena of creep and carbon dioxide attack for durability assessments. The full model comprises one span alone, composed by 14 segments, symmetrically located with

reference to mid-span (Figure 16) and it schematises the real bridge structure shown in Figures 17-19.

The first seven segments were created, applying symmetry boundary conditions only once the two half-spans were connected (closure); in this way the real construction sequence is reproduced, starting from a pier and symmetrically creating two segments, one on each pier side every seven days, hence maintaining equilibrium. The construction practice requires the creation of two additional half-spans both connected to another pier; their closure determines the real bridge span.

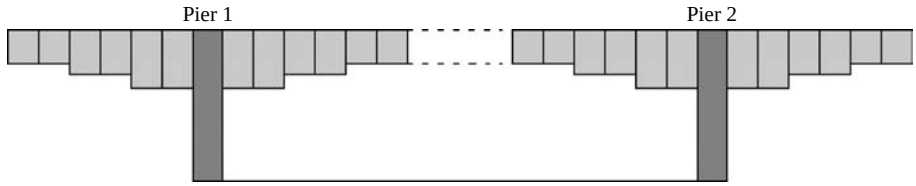

Figure 16.
Commonly used construction sequence for segmental bridges

Figure 17.
The Fadalto bridge, Italy

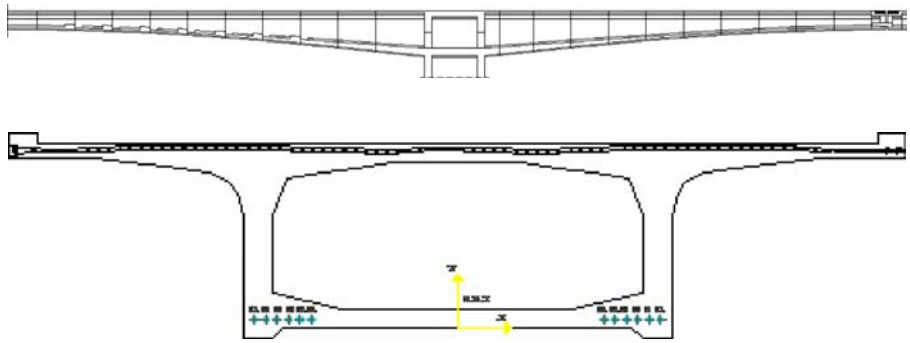

Figure 18.
Typical section of pier and segments

Figure 19.
Section-type

5.1 Model description

About 20-nodes 3D isoparametric finite elements were used; each caisson (Figure 20) was discretized by 11 elements (more elements were used in other analyses), with a total of 132 nodes per caisson.

Once the segment was "activated" dead loads were assigned (Figure 21); after seven days the second segment was introduced (activated) and, contemporaneously, the previous one was tensioned by the continuity tendons (Figure 22), simulated by longitudinal forces applied on the vertical cores; this procedure was repeated for all the seven segments.

Further, the static scheme was changed due to the closure operation (connection between two half-spans, Figure 23), applying symmetry boundary conditions to the last previously-free segment edge.

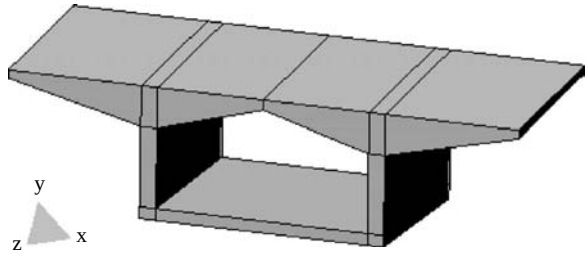

Figure 20.
FE mesh of the caisson-type

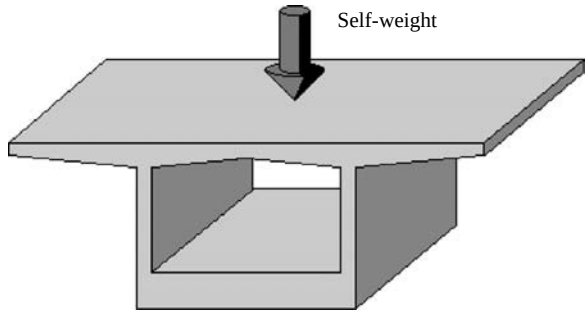

Figure 21.
Dead loads application

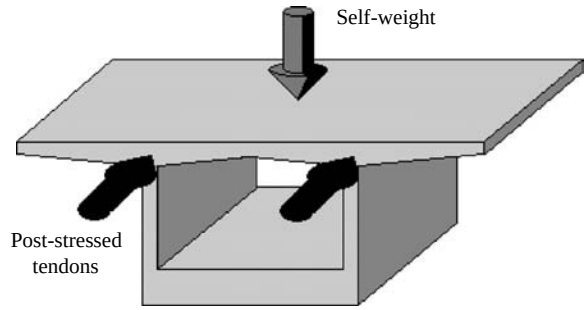

Figure 22.
Application of continuity tendons

To complete the connection, lower post-tensioning cables were applied (Figure 24); the final discretization for the complete bridge half-span is shown in Figure 25. An external "cover" of finite elements was used to reproduce the environmental characteristics in terms of relative humidity, temperature and CO_2 concentration. The external RH was fixed to 55 per cent, whereas each caisson had an initial RH = 99 per cent (saturated conditions). The analysis was pushed up to the bridge's service life span, i.e. 45 years.

5.2 Material

The material data for the adopted concrete and its mixing characteristics are listed in Tables V and VI, respectively.

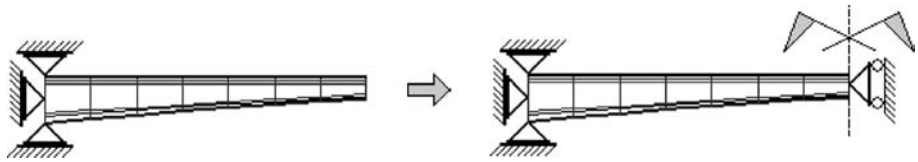

Figure 23.
Change in the static scheme

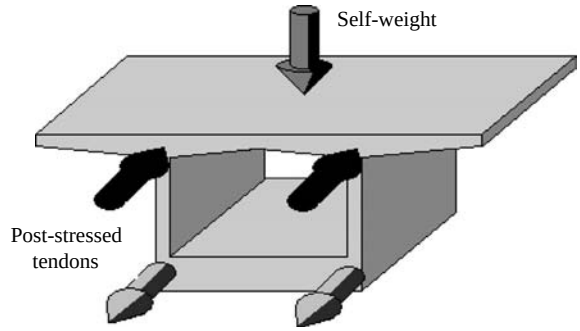

Figure 24.
Final load condition

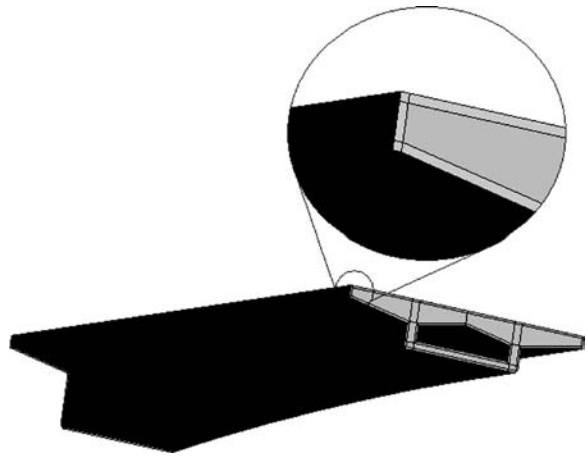

Figure 25.
Final FE mesh for the bridge half-span

5.3 Mesh growing

The accretion sequence is shown in Figure 26: every seven days a new segment is added, up to the closure of the half-span.

5.4 Model results

Figure 27 shows the history of concrete relative humidity up to 49 days: each curve represents the general humidity variation within each segment. Humidity is at a constant value of about 99 per cent until the corresponding segment is activated; then, a slight recovery in humidity for the former caisson – which is drying – is shown: in fact, the curves represent the humidity state at the interface between two adjacent segments, which is changed by the connection with the following segment.

The general trend of humidity for the whole structure is shown in Figure 28: RH decreases with time as concrete dries and desaturates, as shown also in Figure 29 for a typical caisson.

The evolution of settlements, for a node belonging to the first caisson, is shown in Figure 30: the first settlement recoveries are due to the continuity tendons, whose effect predominates on the segments' self-weight; the last jump is given by the lower post-tensioning cables introduced when the static scheme changes, generating a displacement recovery. The final deformed shape for half bridge is shown in Figure 31.

Once the construction sequence is concluded, a carbon dioxide attack is staged with an external CO_2 concentration of 10 per cent, i.e. an accelerated environment (Section 4.1), obtaining the contour maps for carbonation depth of Figure 32 and a typical $CaCO_3$ history of Figure 33: clearly, the referring node belongs to a part of the structure initially not-carbonated (internal).

Figure 34 shows the carbonation profiles within the half section of a typical caisson, after 1,000 days: as stated in Section 4.1, to predict the structure performance under normal conditions for CO_2 attack, the carbonation depth must be reduced by about seven times.

Material property set 2 (segments)	Value
Elastic modulus (MPa)	0.349620×10^{5}
Poisson's ratio	0.200000×10^{0}
Diffusivity X (m/day)	0.150000×10^{2}
Diffusivity Y (m/day)	0.150000×10^{2}
Diffusivity Z (m/day)	0.150000×10^{2}
Unrestrained shrinkage for $H = 0$	-0.400000×10^{-2}
Coeff. r_0 stress for thermal deformations	0.450000×10^{0}

Table V.
Material properties

Symbol	Value	Unit	Species
w	148.5	kg/m^3	Water content
c	450	kg/m^3	Cement
g	951	kg/m^3	Gravel
s	844	kg/m^3	Sand
a	1795	kg/m^3	Aggregates

Table VI.
Concrete mixing

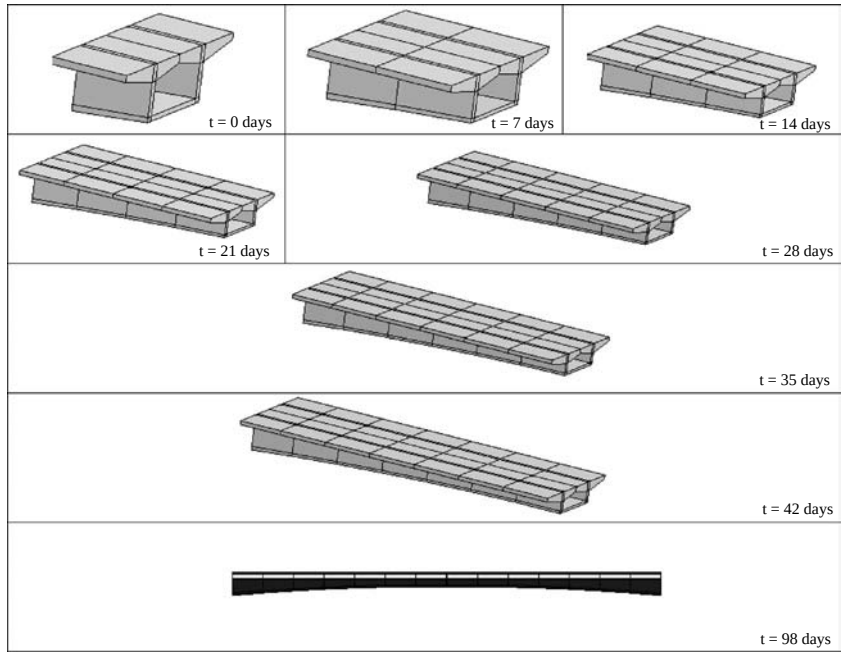

Figure 26.
Mesh accretion

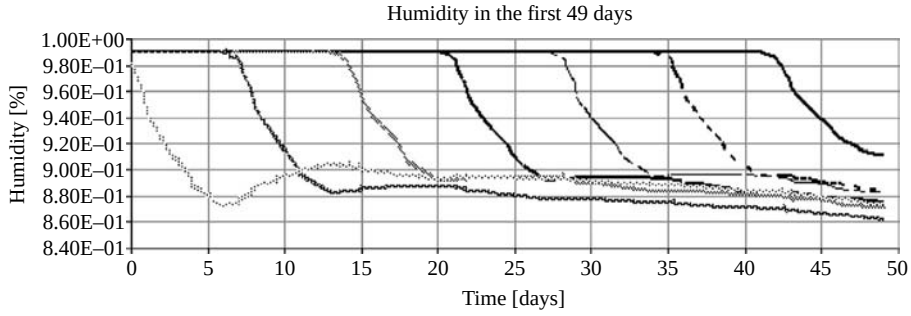

Figure 27.
Humidity variation

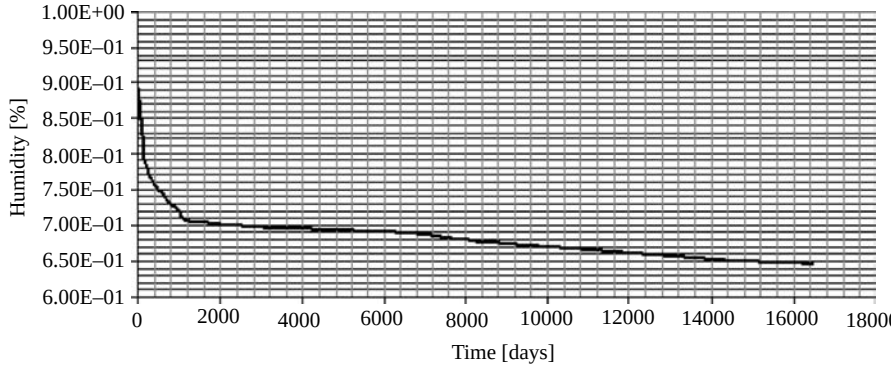

Figure 28.
Humidity history for the whole bridge structure

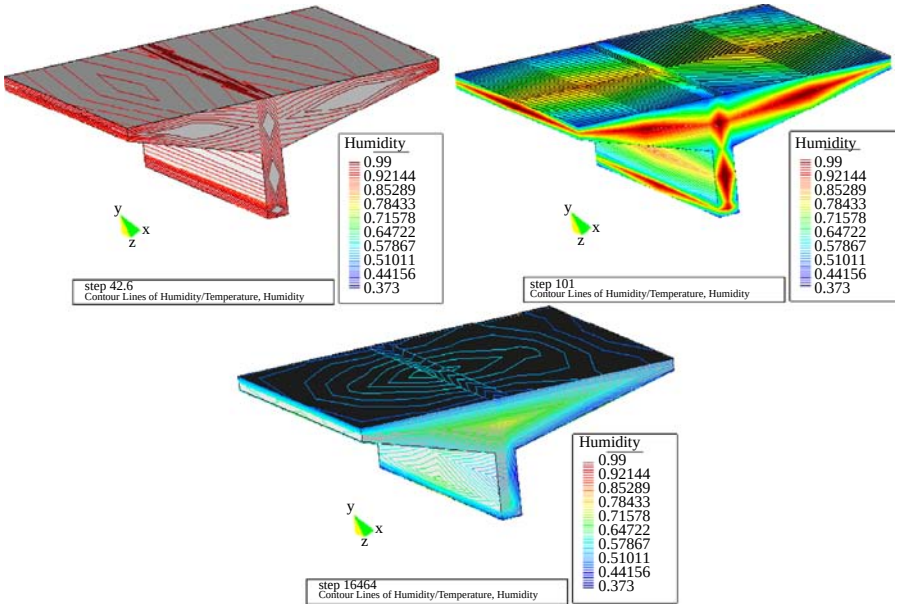

Figure 29.
Contour map of humidity at different time stations

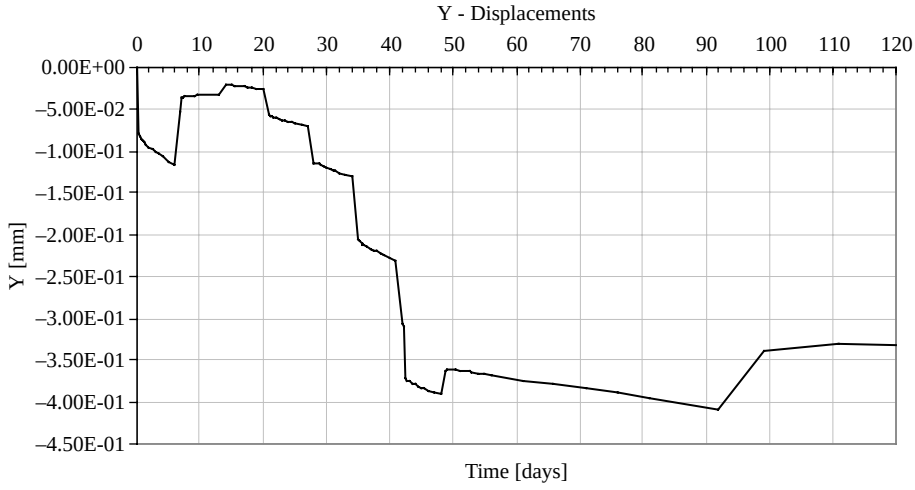

Figure 30.
Settlements history

6. Conclusions

The analysis of a typical 3D segmental bridge made of precast concrete was carried out through a fully coupled thermo-hygro-mechanical F.E. model, taking into account the phenomenon of body accretion, necessary for the simulation of the construction sequence, and carbon dioxide attack. Creep, relaxation and shrinkage effects were included according to the theory developed in the 1970s by Bažant for concretes and geomaterials. The porous material was modelled by n Maxwell elements in parallel (Maxwell-chain model).

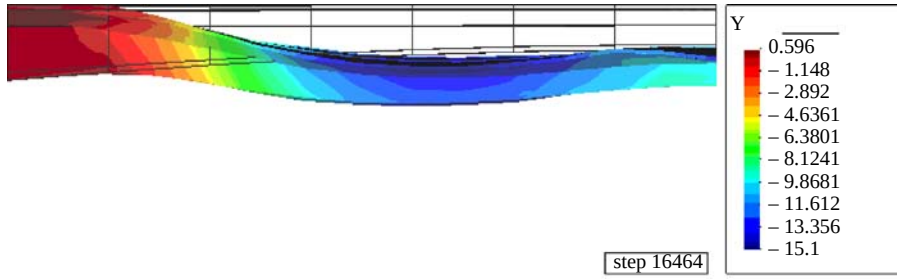

Figure 31.
Final deformed shape

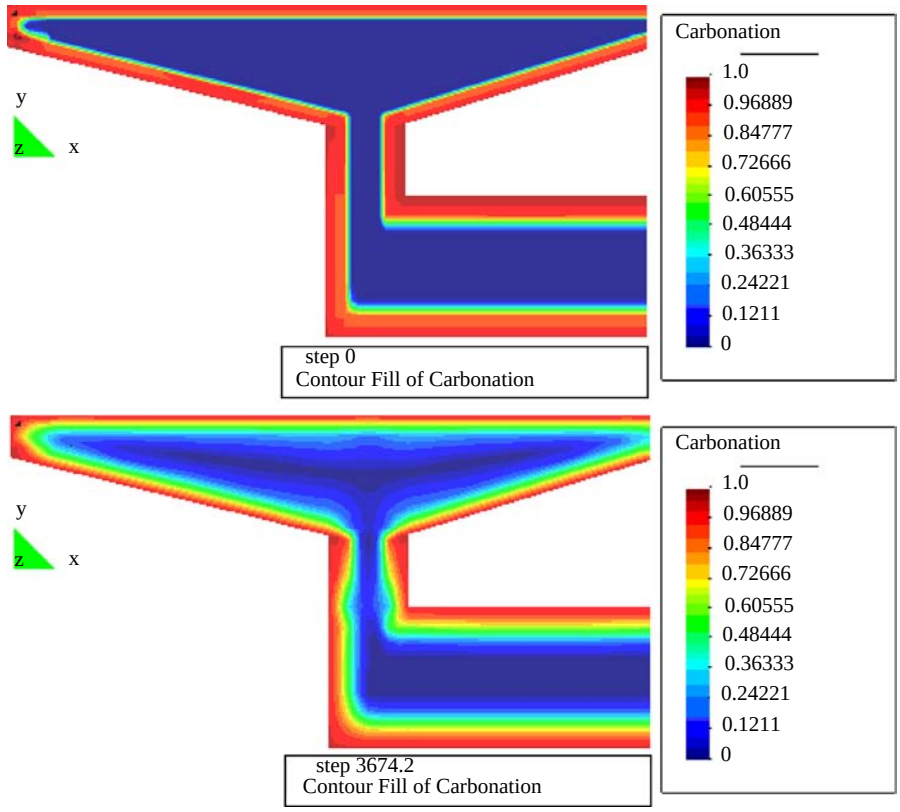

Figure 32.
Carbonation depth at different times

The rate-type approach will be updated in a future paper following the lines of both the solidification and the relaxation of microprestress theories.

First, calibration analyses were developed to check the 3D model capabilities for predicting carbonation phenomena within the concrete material. 3D analyses allowed for effectively considering transversal effects, so that the structural response is more accurately predicted if compared to 1D and 2D analyses. Severe conditions for CO_2 attack were considered for assessing the durability of the segmental bridge at the end

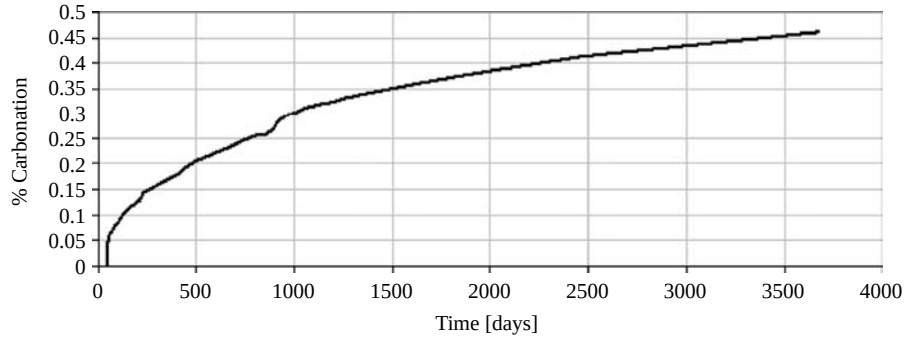

Figure 33.
Carbonation history at a typical caisson's core

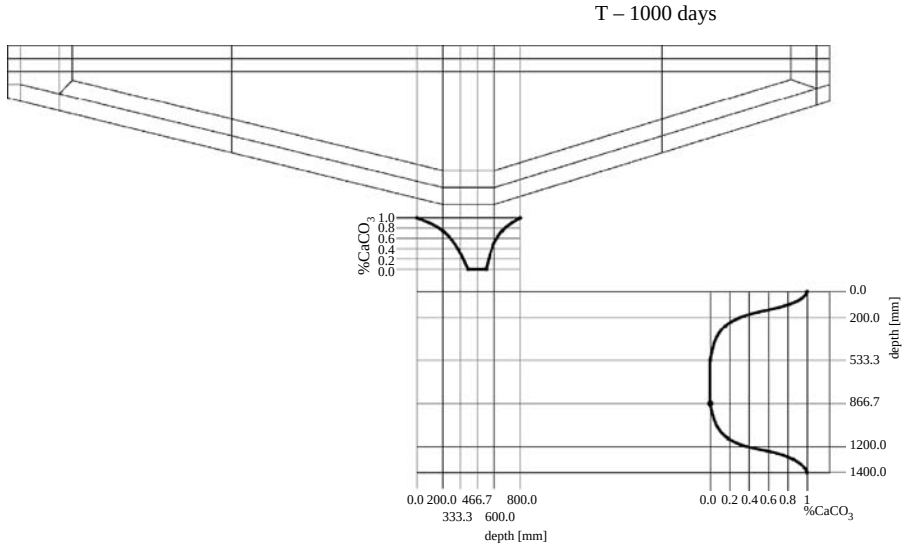

Figure 34.
Carbonation profiles within half section of a caisson

of the construction sequence, when drying and creep phenomena are still developing. A durability assessment depends on environmental conditions, concrete mixing and transport interactions; in fact CO_2 transport is driven by a time-varying carbon dioxide diffusivity coupled with water diffusivity, due to the carbonation process affecting concrete's micro pore structure (i.e. porosity/permeability). A carbon dioxide diffusion history was taken in accordance with available experimental tests for comparison purposes and the full 3D structure was further modelled to asses the durability of the bridge under an accelerated environment.

References

Arutiunian, N.Kh. (1976a), "On the theory of creep for nonuniformly aging media", *Akademii Nauk SSSR*, Vol. 229 No. 3.

Arutiunian, N.Kh. (1976b), "On the equation of state in the nonlinear theory of creep of nonuniformly aging bodies", *Doklady Akademii Nauk SSSR*, Vol. 231 No. 3.

Arutiunian, N.Kh. (1977), "Boundary value problem of the creep for a body with accretion", *Journal of Applied Mathematics and Mechanics*, Vol. 41 No. 5, pp. 804-10.

Bažant, Z.P. (1972a), "Numerical determination of long-range stress history from strain history concrete", *Materials and Structures*, Vol. 5 No. 3, pp. 135-41.

Bažant, Z.P. (1972b), "Prediction of concrete creep effects using age-adjusted effective modulus method", *Journal of the American Concrete Institute*, Vol. 69, pp. 212-7.

Bažant, Z.P. (1979a), "Physical model for steel corrosion in concrete sea structures – theory", *Journal of the Structural Division*, Vol. 105, No. ST6, pp. 1137-53.

Bažant, Z.P. (1979b), "Physical model for steel corrosion in concrete sea structures – Application", *Journal of the Structural Division*, Vol. 105, No. ST6, pp. 1155-66.

Bažant, Z.P. (1982), "Input of creep and shrinkage characteristics for a structural analysis program", *Materials and Structures*, Vol. 15 No. 4, pp. 283-90.

Bažant, Z.P. (1988), *Mathematical Modeling of Creep and Shrinkage of Concrete*, Wiley, Chichester.

Bažant, Z.P. (2001), "Creep of concrete", in Buschow, K.H.J. et al. (Eds), *Encyclopedia of Materials: Science and Technology*,Vol. 2C, Elsevier, Amsterdam, pp. 1797-800.

Bažant, Z.P. and Kim, J.K. (1991), "Improved prediction model for time-dependent deformations of concrete: part 2: basic creep", *Materials and Structures*, Vol. 24 No. 6, pp. 409-21.

Bažant, Z.P. and Prasannan, S. (1989a), "Solidification theory for concrete creep. I: formulation", *Journal of Engineering Mechanics*, Vol. 115 No. 8, pp. 1691-703.

Bažant, Z.P. and Prasannan, S. (1989b), "Solidification theory for concrete creep. II: verification and application", *Journal of Engineering Mechanics*, Vol. 115 No. 8, pp. 1704-25.

Bažant, Z.P. and Wittmann, F.H. (1982), *Creep and Shrinkage in Concrete Structures*, Wiley, Chichester.

Bažant, Z.P. and Wu, S.T. (1974), "Rate type creep law of aging concrete based on Maxwell chain", *Materials and Structures*, Vol. 7 No. 37, pp. 45-60.

Bažant, Z.P. and Xi, Y. (1993), "Continuous retardation spectrum for solidification theory of concrete creep", *Journal of Engineering Mechanics*, Vol. 121 No. 2, pp. 281-8.

Bažant, Z.P. and Xi, Y. (1994), "Drying creep of concrete: constitutive model and new experiments separating its mechanism", *Materials and Structures*, Vol. 27 No. 1, pp. 3-14.

Bažant, Z.P. and Zi, G. (2002), "Continuous relaxation spectrum for concrete creep and its incorporation into microplane model M4", *Journal of Engineering Mechanics*, Vol. 128 No. 12, pp. 1331-6.

Bažant, Z.P., Hauggaard, A.B., Baweja, S. and Ulm, F.J. (1997), "Microprestress-solidification theory for concrete creep. I: aging and drying effects", *Journal of Engineering Mechanics*, Vol. 123 No. 11, pp. 1188-94.

Bugakov, I.I. (1973), *Creep in Polymer Materials*, Nauka, Moscow.

Collepardi, M. (1980), *Scienza e Tecnologia del calcestruzzo*, Hoepli Ed., Milan (in Italian).

Diatlovitskii, L.I. and Vainberg, A.I. (1975), *Formation of Stresses in Gravity Dams*, Naukova Dumka, Kiev.

Houst, Y.F. and Wittmann, F.H. (1994), "Influence of porosity and water content on the diffusivity of CO_2 and O_2 through hydrated cement paste", *Cement and Concrete Research*, Vol. 24 No. 6, pp. 1165-76.

Ishida, T., Maekawa, K. and Soltani, M. (2004), "Theoretically identified strong coupling of carbonatin rate and thermodynamic moisture states in micropores of concrete", *Journal of Advanced Concrete Technology*, Vol. 2 No. 2, pp. 213-22.

Majorana, C.E. (1985), "Numerical simulation of drying and shrinkage of concrete with a multiphase inhomogeneous material model", Technical report, Istituto di Scienza e Tecnica della Costruzioni, Università di Padova, Padova.

Majorana, C.E. and Salomoni, V.A. (2004), "Parametric analyses of diffusion of activated sources in disposal forms", *Journal of Hazardous Materials*, Vol. A113, pp. 45-56.

Majorana, C.E. and Vitaliani, R. (1990), "Numerical modelling of creep and shrinkage of concrete by finite element method", *Proc. 2nd Int. Conf. on Computer Aided Design in Concrete Structures SCI-C*, pp. 773-84.

Majorana, C.E., Salomoni, V. and Schrefler, B.A. (1998), "Hygrothermal and mechanical model of concrete at high temperature", *Materials and Structures*, Vol. 31, pp. 378-86.

Majorana, C.E., Salomoni, V. and Secchi, S. (1997), "Effects of mass growing on mechanical and hygrothermic response of three-dimensional bodies", *Journal of Materials Processing Technology*, Vol. PROO64/1-3, pp. 277-86.

Naumov, V.E. (1994), "Mechanics of growing deformable solids: a review", *Journal of Engineering Mechanics*, Vol. 120 No. 2, pp. 207-20.

Papadakis, V.G., Vayenas, C.G. and Fardis, M.N. (1991), "Fundamental modeling and experimental investigation of concrete carbonation", *ACI Materials Journal*, Vol. 88 No. 4, pp. 363-73.

Saetta, A.V., Schrefler, B.A. and Vitaliani, R. (1993), "The carbonation of concrete and the mechanism of moisture, heat and carbon dioxide flow through porous materials", *Cement and Concrete Research*, Vol. 23, pp. 761-72.

Saetta, A.V., Schrefler, B.A. and Vitaliani, R. (1995), "2-D model for carbonation and moisture/heat flow in porous materials", *Cement and Concrete Research*, Vol. 25 No. 8, pp. 1703-12.

Schrefler, B.A., Simoni, L. and Majorana, C.E. (1989), "A general model for the mechanics of saturated-unsaturated porous materials", *Materials, Structures*, Vol. 22, pp. 323-34.

Tschoegl, N.W. (1971), "A general method for the determination of approximations to the spectral distributions from the transient response functions", *Rheologica Acta*, Vol. 10, pp. 595-600.

Tschoegl, N.W. (1989), *The Phenomenological Theory of Linear Viscoelastic Behaviour*, Springer-Verlag, Berlin.

van der Veen, T. (2003), "Time-dependent effects in concrete segmental bridges", *Bridgeline*, Vol. 12 No. 2, pp. 5-6.

Widder, D.V. (1971), *An Introduction to Transform Theory*, Academic Press, New York, NY.

Corresponding author
Valentina A. Salomoni can be contacted at: salomoni@dic.unipd.it